

Aeolian megaripple stripes: Supplementary material

Tyler Gough¹, Chris Hugenholtz¹, Thomas Barchyn¹

¹Department of Geography, University of Calgary, 2500 University Dr NW, Calgary, AB T2N 1N4

WAVELENGTH MEASUREMENTS

Wavelength measurements were completed at a number of megaripple stripe locations (see Table 1 in the main text). The satellite imagery provided an overview of the striped pattern and allowed for measurement of megaripple wavelengths. The imagery spatial resolution was, in all terrestrial cases, insufficient to resolve specific details about smaller bedform corridor morphology. The high-resolution imagery and size of the features at Rabe Crater, Mars allowed features in both corridor types to be measured. The only sites for which no morphometrics whatsoever were resolved in satellite imagery with enough detail were the Oceano Dunes and Dillon Beach, California.

An approach developed for quantifying the spacing of sorted stripes on hillslopes was adapted for measuring megaripple wavelengths in downwind and crosswind directions (Francou et al., 2001). Figure S1 illustrates the dimensions representing crosswind and downwind wavelengths of the megaripple stripes. With the exception of the megaripple stripes at Oceano Dunes, which were measured in the field with a tape measure, wavelength measurements were made using Google Earth imagery and a HiRISE image of Mars. Images were imported into ArcMap© and georeferenced using 15–23 tie points and coordinates from Google Earth (WGS84). To limit bias, a random sampling approach was applied in which a polygon sampling area was drawn over the megaripple stripes and random points were generated within the sampling area. Sample points ranged from 24 for the site with the least extensive megaripple stripes (Namibia) to 103 for the site with the most extensive megaripple stripes (Argentina). Transects were then drawn to measure crosswind and downwind wavelength. Downwind transects were created perpendicular to crestline orientation, beginning at the crest of the feature closest to the sampling point and ending at the crest of a feature downwind in the same corridor as the first feature. The downwind wavelength was measured as transect length divided by the number of crestlines crossed by the transect, not including the first. All transects began and ended on a crestline. Crosswind transects were drawn parallel to the orientation of megaripple crestlines such that they intersected the sampling point and crossed the spanwise width of several

megaripple stripes. Crosswind wavelength was measured as transect length divided by the number of pairs of megaripple and smaller bedform corridors intersected. Many sampling points fell in locations where the wavelength could not be determined. In these cases, the nearest location that could be resolved was used. The mean wavelength for each location was calculated by dividing the sum length of all transects by the sum number of wavelengths counted for all transects.

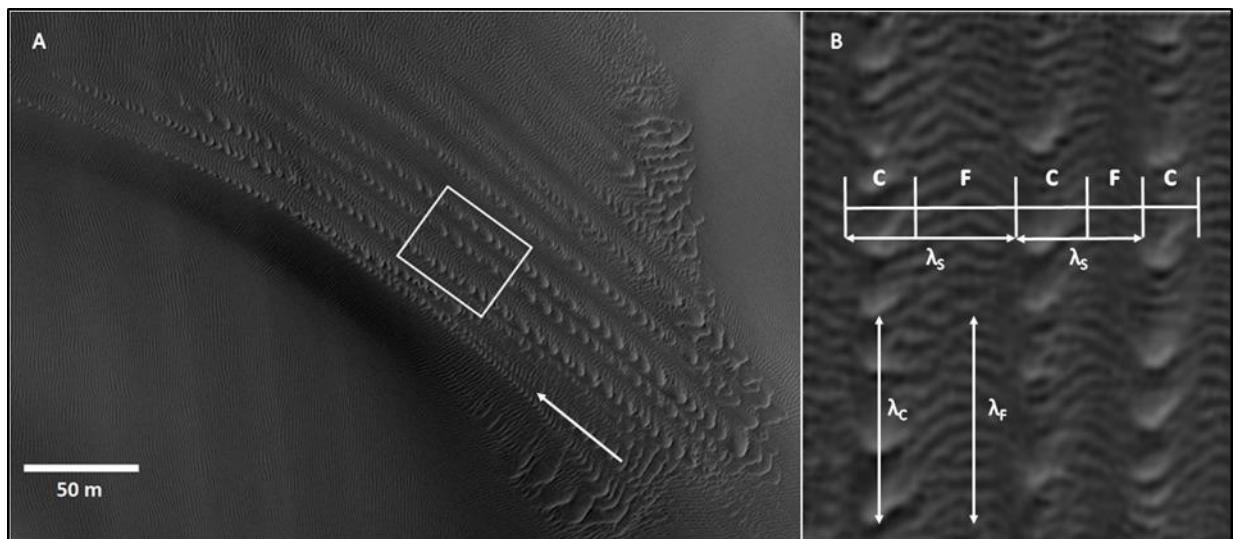


Figure S1: (A) Overview of megaripple stripe pattern in the Rabe Crater dune field, Mars. Arrow indicates assumed dominant direction of transport. (B) Inset image showing alternating pattern of megaripple corridors, C, and smaller bedform corridors, F. A spanwise wavelength, λ_s , is defined as the width of a pair of corridors. The two downwind transects show λ_C , where the transect spans three wavelengths, and λ_F , where the transect spans ten wavelengths over the same distance. (Image: HiRISE PSP_002824_1355, NASA/JPL/University of Arizona).

Wavelength measurements made at each site were shown in Table 1 of the main text. The megaripple corridors at most locations have downwind wavelengths of 2 to 3 metres, with much larger features present at Abra Pomez and Mars. Wavelengths of the smaller bedforms were measured from imagery for Mars and in the field for the Oceano Dunes.

The data suggest the crosswind wavelength of megaripple stripes is approximately two times larger than the downwind wavelength of megaripple corridors (Figure S2). A simple linear regression for terrestrial and Martian stripes yields an R^2 of 0.97 for these data, but further data and field research are required to test and reinforce this relationship. This is especially true given

that there is a paucity of data for megariipple stripes that are too small to resolve in satellite imagery (i.e., wavelengths < 2 m). An important caveat to results in Table 1 is that downwind wavelengths estimated from satellite imagery are likely an overestimation because some crestlines may not be detectable in imagery. Further, there is spatial variability in crosswind and downwind wavelengths throughout the megariipple stripes and the 2:1 ratio is only representative as an average; it is premature to suggest this ratio is broadly indicative of an ‘ideal’ or ‘stable’ form of the pattern. The average coefficients of variation of downwind and crosswind wavelengths measured from imagery were 0.17 and 0.18, respectively. This suggests that although there is a larger range of values for the spanwise wavelengths (0.9–28.5 m) than the downwind megariipple wavelengths (0.3–8.8 m), the relative variability of downwind and crosswind wavelengths is virtually the same.

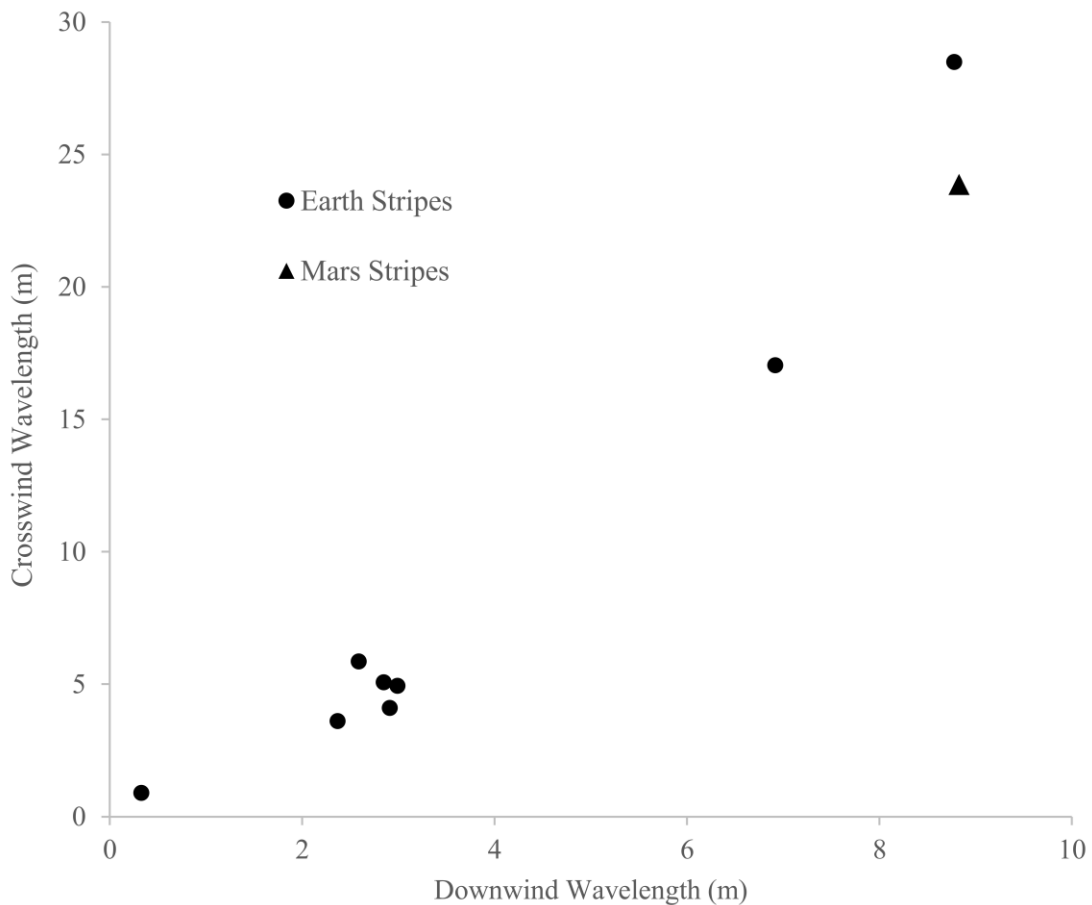


Figure S2: Averaged crosswind and downwind (megariipple corridor) wavelengths of measured megariipple stripes on Earth and Mars.

GRAIN SIZE ANALYSES

Grain size analyses were performed for megaripple stripes at the Oceano Dunes, USA, and at Abra Pomez, Argentina to understand and make further distinction between corridors of megaripples and corridors of smaller bedforms. There are several methods for quantifying grain size. Each is used depending on whether a physical sample is available or not, and the nature and size of that sample. For Oceano Dunes, a laser diffraction analysis method was used on physical samples collected in the field. For Abra Pomez, a photo-based method was used from close-range photographs taken of the surface during field campaigns at the site, because collecting physical samples was not possible at the time.

OCEANO DUNES, CALIFORNIA, USA

Sediment samples were acquired for grain size analysis from the Oceano Dunes in November 2017 at four sampling sites. Samples were acquired from crests of bedforms in both corridor types and in transitional areas between the two (Figure S3). Ripple crests and stoss slopes were targeted for sampling. In total, 17 samples were obtained from megaripple corridors, 13 samples from smaller bedform corridors, and five from transitional areas. Surface samples (< 0.5 cm) and depth samples (1-5 cm) were acquired to assess armor grain size and bulk grain size of the bedforms. The surface samples were collected by scraping near-surface sediment with a spoon, penetrating no farther than approximately a half centimeter below the surface. Bulk samples were acquired to a depth of 1-5 cm (from the crest of the ripple to its base) using a spoon. Sample mass ranged from 38 to 110 g at each location, and each sample contained material from several bedforms, typically five to twenty, in the same corridor. In total, nine surface samples and 26 depth samples were acquired.

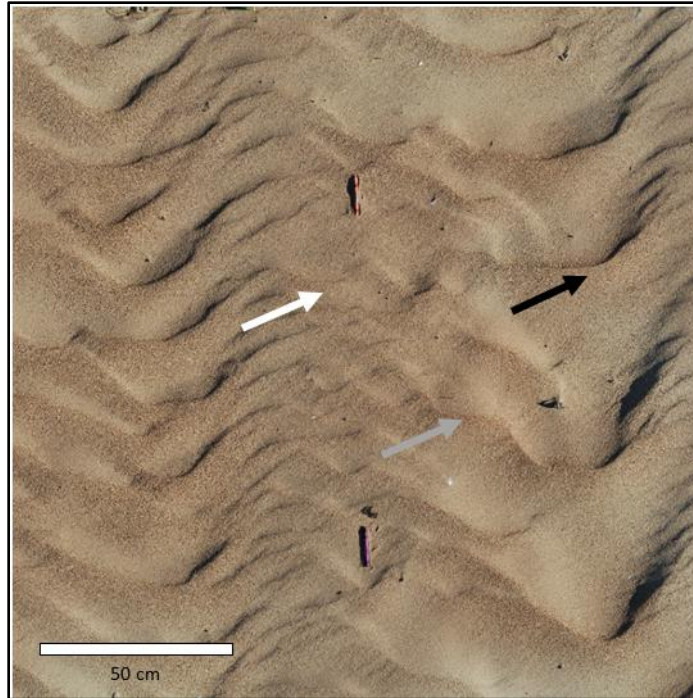


Figure S3: Example locations of sample acquisition for megaripple corridors (black), smaller bedform corridors (white), and transitional areas (grey) for sample acquisition. As noted in the text, several bedforms were used to gain a sufficient sample mass and representative sample.

Each sample was riffled and two subsamples from each sample were measured using a Hydro 2000G sample dispersion unit and a Malvern Mastersizer 2000© laser particle size analyzer (LPSA) with a standard operating procedure (Viton and Sadler, 1997). Prior to measurement, organic material was removed from each sample using a hydrogen peroxide solution and was deflocculated using a sodium hexametaphosphate solution. Although there was virtually no organic material or particles smaller than fine sand, these steps were taken to ensure that guidelines were followed for all samples. The Mastersizer 2000© LPSA is capable of measuring particles ≤ 2 mm. No grains > 2 mm were present in any of the samples. Grain sizes were calculated by the LPSA volumetrically and binned into narrow grain size ranges. This generates a probability density for each grain size range from which GSD properties are determined.

Grain size data for surface and depth samples of megaripple stripes at the Oceano Dunes were aggregated to the level of megaripple corridors and smaller bedform corridors (Table S1). The results of a two-sample t-test and a Mann-Whitney U test between the means of all

megaripple corridor and smaller bedform corridor samples confirm a statistically significant difference in grain size between corridor types for both surface and depth samples with $p < 0.01$. This grain size distinction was observed at all four sampling sites.

Examples of the typical distributions observed in the samples are shown in Figure S4A. For both corridor types, surface samples were found to be coarser than depth samples. This is expected in megaripples, where coarsening is observed with smaller sampling depths (Yizhaq et al., 2012a). This suggests that features in smaller bedform corridors have some megaripple characteristics (i.e., armouring) despite their smaller wavelengths. Depth samples generally have a larger standard deviation and range than surface samples. Importantly, only three of the seventy samples show a bimodal distribution, with all other samples being distinctly unimodal and largely log-normally distributed. This does not reflect what has typically been reported for megaripples, where it is often stated that a bimodal GSD is required for their formation. As addressed by Lämmel et al. (2018), only poorly sorted grains may be required for the initiation of megaripples. Although only three samples show a bimodal distribution, the distribution of sample means (Figure S4B) for depth samples is non-normally distributed and multimodal. This suggests local variability in grain size.

TABLE S1. AGGREGATED GRAIN SIZE STATISTICS FROM OCEANO DUNES

Sample Type	n	Mean	D ₁₀	D ₅₀	D ₉₀	Std. Dev.
Megaripple (Depth)	22	713	346	665	1146	82
Megaripple (Surface)	12	724	416	688	1080	46
Smaller Bedform (Depth)	20	393	188	353	660	108
Smaller Bedform (Surface)	6	575	325	541	876	36
Transition (Depth)*	10	273	160	251	403	52

Note: All grain sizes presented are in μm .

*Transition area samples were acquired at only two of four sampling sites. Although grain sizes for the transition areas are smaller than smaller bedform corridors in aggregate, the transition areas are coarser than smaller bedform corridor samples from their respective sampling sites.

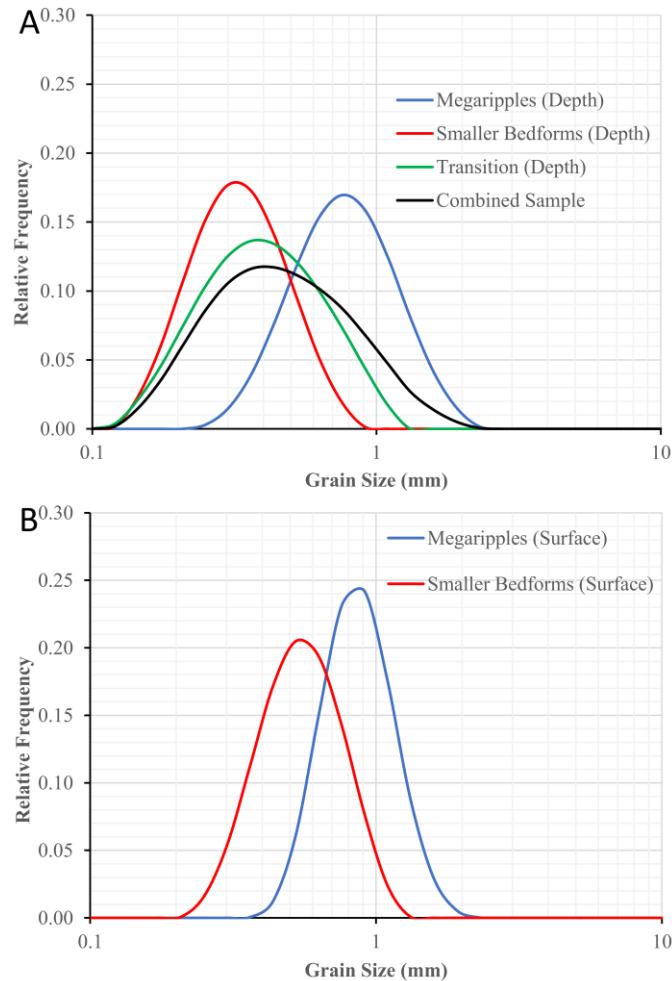


Figure S4: Grain size curves for a series of megaripple stripe samples at the Oceano Dunes, California. (A) Three samples acquired at depth from stoss slopes and crests of bedforms in megaripple corridors, smaller bedform corridors, and transitional areas. Their combined distribution is also shown. (B) Two samples acquired at the surface of bedforms in the same location as (A) for the megaripples and smaller bedforms.

ABRA POMEZ, ARGENTINA

Close-range images of megaripple and smaller bedform corridor surface sediment were acquired at Abra Pomez with a consumer-grade camera in 2014 and 2015. The images were taken at a height of approximately 20 cm above the surface and slightly stossward of crests to limit geometric distortion. A ruler was positioned in each image for scaling. Each image was calibrated using OpenCV image calibration software to correct for the slight fisheye effect inherent in most consumer-grade digital cameras. The location of each image from Abra Pomez is shown in Figure S5A. The method of extracting measurements of grain diameter from images is referred to as ‘photosieving’ (Ibbeken, 1986). There are many different photosieving techniques, including some that are fully automated (e.g., Rubin, 2004; Buscombe, 2013). However, these automated methods can have large errors. In this study, a manual technique was applied whereby metrics were extracted from digitized grain perimeters visible in the images.

To minimize sampling bias in the photosieving process, a random sampling approach was used where random points were generated on each image and a buffer was generated around each point. Grain perimeters were digitized if any portion of the grain was located inside the buffer area (Figure S5B). The radius of buffers was set to 75 pixels for images from smaller bedform corridors and 100 pixels for images from megaripple corridors. Three to ten buffers were used per image. Total grains digitized per image ranged from 95 to 743. In total, 43 images were used for digitizing: 34 images from the 2015 photo survey and 9 from the 2014 photo survey. This method generated a dataset of 9780 grains: 5518 grains from megaripple corridors and 4262 grains from smaller bedform corridors.

Grain dimensions were extracted from the polygons using ArcGIS© software. The grain size being reported is the width of a minimum bounding rectangle capable of containing the digitized polygon. The length of the rectangle can be interpreted as describing the grain’s primary axis of and its width the secondary or b-axis. As grain size is typically measured as the latter (i.e., sieve size) by most methods, the b-axis width is reported as grain size here.

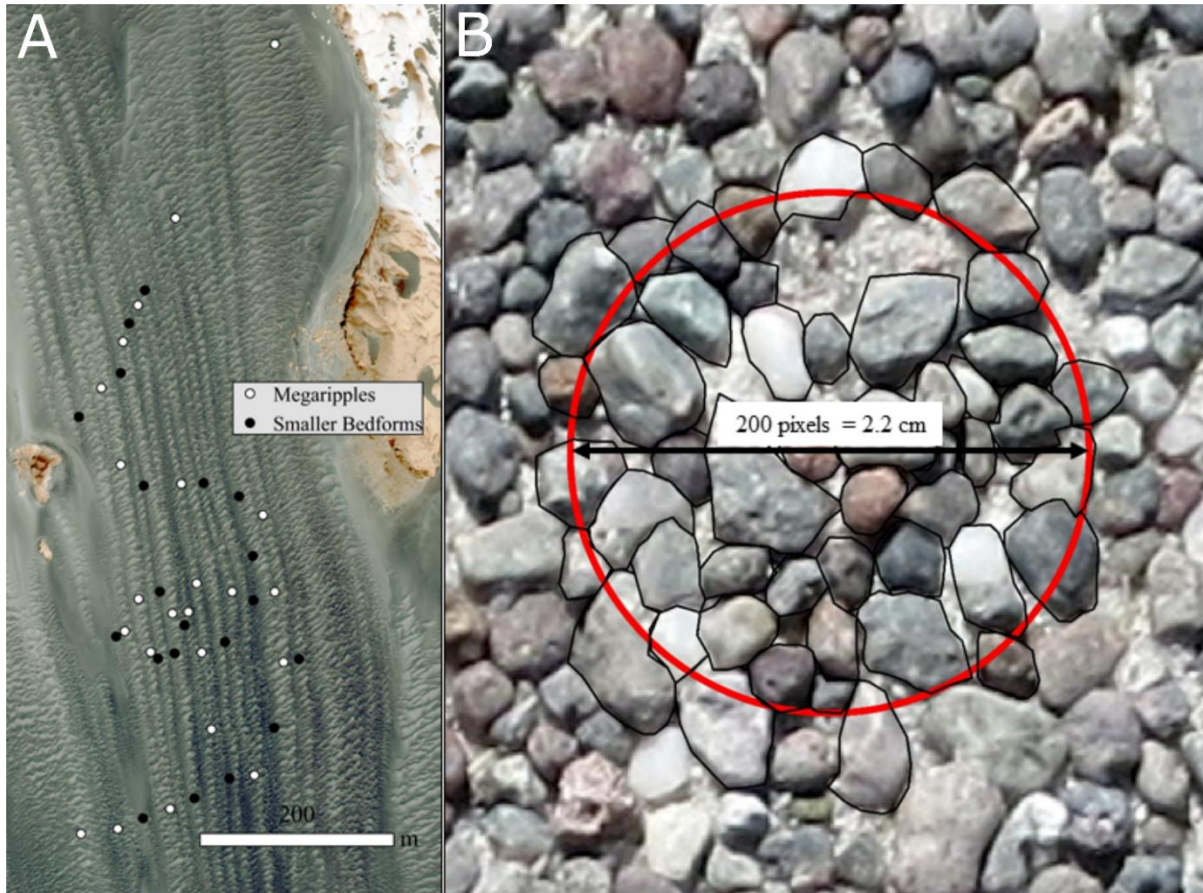


Figure S5: (A) Locations of the 43 images used for photosieving (23 from megaripple corridors and 20 from smaller bedform corridors). (B) Example of a buffer and polygon-drawing method used for photosieving of a megaripple stoss slope image with a buffer diameter of 200 pixels.

The photosieving method used here is more complex than many other manual methods. Most methods task the user with simply estimating the intermediate axis with a digitized line. However, drawing polygons and automating axis calculation likely eliminates a significant portion of user bias and is capable of outputting other geometric features of the grains, including their long axis, surface area, and the axis orientation of the axes. These geometric features could be used to generate estimates of roundness or orientation of grains that may be of value in other applications.

As with the Oceano Dunes, megaripple stripes in Argentina show a distinct sorting of grain size between megaripple and smaller bedform corridors. Results from the photosieving analysis are shown in Table S2 and Figure S6. As the photosieving data for both the smaller bedforms and the megaripples are non-normally distributed and data were generated for

individual grains, a Mann-Whitney U test was used to compare the two corridor types from Argentina. This test confirms that there is a statistically significant difference between the megaripple grain sample and the smaller bedform grain sample with $p < 0.01$.

A bimodality is apparent in the aggregated GSD of megaripple samples, but not in the GSD of smaller bedforms. Of all the sample images, 14 of 23 megaripple images and 5 of 20 smaller bedform images showed bimodal or multimodal distributions. The sample distribution of photosieved results was shown in Figure 1E of the main text and reveals a similar separation, but less complete than Oceano, of sample D_{50} distributions between corridor types. As will be discussed below, it is doubtful these photosieved grain sizes are directly comparable to those collected via physical sampling. It is estimated that the minimum grain size capable of being digitized reliably in these images was 0.5 mm, with some variability between images. Although most of the grains in images were resolvable, several pockets of what appeared to be small grains could not be digitized. Therefore, the left tails of distributions presented in Figure S6 are not representative. The reliability of photosieving increases with larger grains and it is therefore likely that the right tails of these distributions are representative.

TABLE S2. CORRIDOR STATISTICS FROM ABRA POMEZ

Corridor Type	Mean	Standard Deviation	D_{16}	D_{50}	D_{84}	D_{95}	Graphic Skewness
Smaller Bedforms	1.66	0.91	0.79	1.45	2.61	3.38	0.14
Megaripples	2.58	1.21	1.17	2.62	3.77	4.54	-0.06

Note: Values in mm. Results from photosieving of surface grains.

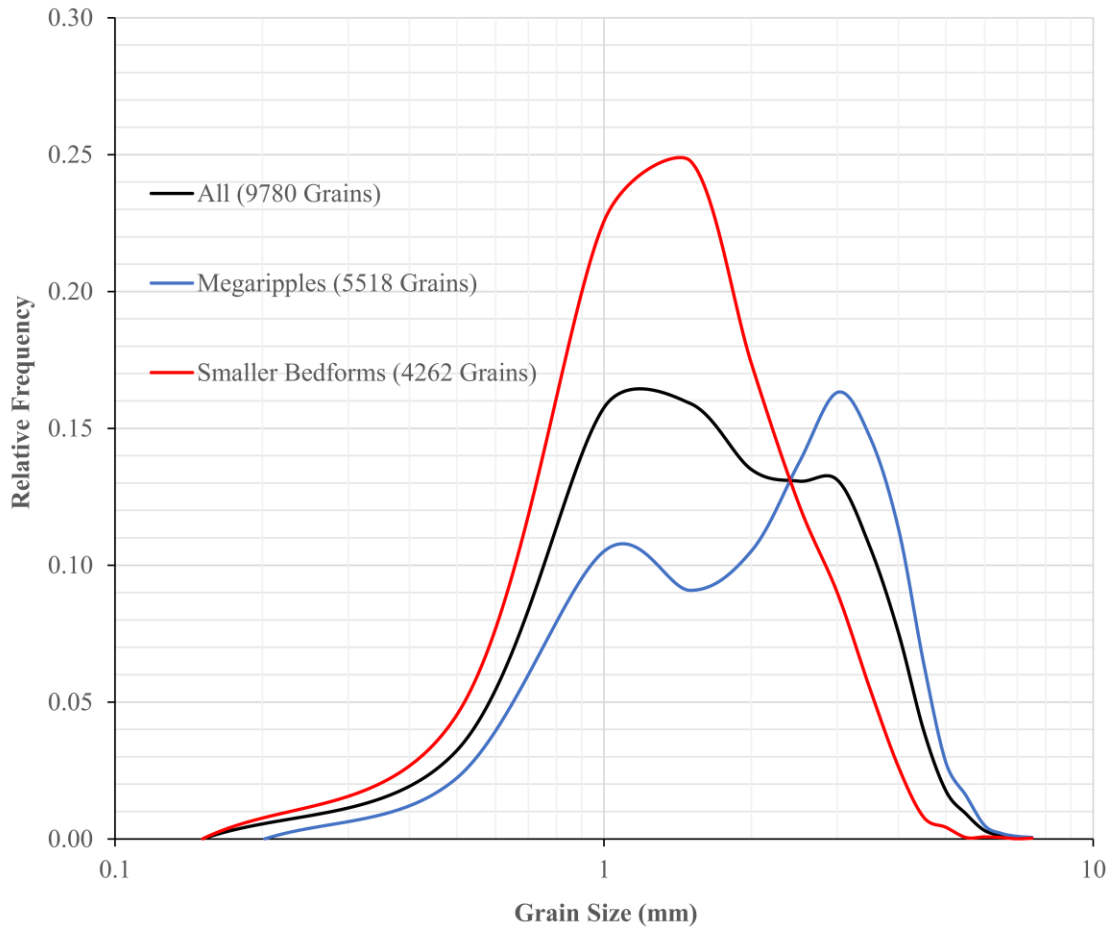


Figure S6: Probability density of grain sizes from photosieving for the megaripples, smaller bedforms, and all grains combined.

COMMENT ON COMMENSURABILITY OF PHOTOSIEVING DATA

Understanding the GSD of aeolian bedforms is crucial because grain size is a primary factor governing morphometrics and transport behaviour. In the case of megaripple stripes, quantifying the grain size difference between corridors of megaripples and smaller bedforms is central to hypotheses outlined in the main text.

It is important to clarify that grain size data derived from photosieving are an approximation of the true grain size. Digitized grain boundaries are not the actual grain boundaries because there are several confounding factors: shadowing, pixel size, imbrication of grains, packing, and other issues (e.g., O’Brien and McKenna Neuman 2018). Therefore, photosieved grain size is relative. It is recognized that the use of photo-based and laser diffraction methods in combination makes direct comparison between grain size at the two field sites difficult. However, the objective of this research is to quantify only the relative difference

between corridor types at individual sites; cross-site comparisons of grain size are a future research objective.

A secondary benefit to using a photo-based method is that it allowed for an evaluation of photo-based grain size analysis, as these methods are growing in popularity and increasingly being used to quantify grain size on Mars from rover images (e.g., Jerolmack et al., 2006, Weitz et al., 2018). As in Jerolmack et al., (2006), GSDs presented for Abra Pomez are based on grain counts rather than mass or volume. This was done because estimating the mass distribution of grains in Argentina is impossible due to the varying densities of surface grains. The region's complex geology means that grains being transported are of varying densities, including pumices $< 1000 \text{ kg/m}^3$ and basalt grains $\sim 3000 \text{ kg/m}^3$ (de Silva et al., 2013). This presents an enormous complication in understanding the region's aeolian transport (Hugenholtz et al., 2015). The complexity of aeolian transport in areas with multiple lithologies is under-researched, and the simplifying assumption of equal densities is often made despite the inaccuracies that such an assumption introduces. For this reason, even if physical samples were available from megaripple stripes in Argentina, a direct comparison between the primarily quartz samples from Oceano and those collected in Argentina would not be feasible because of different grain densities in each sample. Finally, although the photosieving method used may be incommensurable with other methods, it does provide an estimate of surface grain size, preserves original orientation and structure of the bedform surface, and is essential for evaluating a GSD when no other data or samples are available.

3D RECONSTRUCTIONS AND BEDFORM MORPHOLOGY

3D reconstructions of stripes at the Oceano Dunes were created in order to examine vertical characteristics of stripes in detail. DSMs were developed using images from a consumer-grade DSLR camera and Pix4D© software. Five reconstructions, each using 200–600 overlapping photos taken during a November 2017 field campaign, were created to generate DSMs and cross-sectional measurements of ripple profiles. Pix4D© uses principles of structure-from-motion photogrammetry to generate matching points in overlapping imagery (Westoby et al., 2012). Using known ground control points in the photographs, these point cloud outputs can be scaled to produce orthoimages and DSMs. The DSMs were used to evaluate verisimilitude of model simulations. This involved creating transect profiles of megaripple and smaller bedform corridors from the DSM using the 3D Analyst package in ArcGIS©.

Morphometrics calculated from transects taken from four DSMs are shown in Table S3. Mean bedform heights and wavelengths measured from megaripple corridors were approximately triple and double that of smaller bedform corridors, respectively. Additionally, variability observed in bedform heights and wavelengths of megaripple corridors was greater than that observed in smaller bedform corridors. This larger variability is typical of megaripples (Yizhaq et al., 2009; Yizhaq et al., 2012b). Although there are evidently different dominant scales of bedforms present in each corridor, there are bedforms of an intermediate size (10–20 cm) with megaripple characteristics present in both corridor types. The presence of these intermediate forms is likely a consequence of an incomplete sorting of grains between corridors and provides evidence for a continuum of bedform types rather than two distinct classes (impact ripples vs. megaripples) with strictly defined properties.

TABLE S3. CORRIDOR STATISTICS FROM OCEANO DUNES

	Smaller Bedforms (n = 82)	Megaripples (n = 58)
<u>Wavelength</u>		
Mean	10.65	20.40*
Standard Deviation	3.20	8.36
Coefficient of Variation	0.30	0.41
Max.	20.10	43.59
<u>Height</u>		
Mean	0.39	1.40
Standard Deviation	0.11	0.62
Coefficient of Variation	0.28	0.44
Max.	0.74	3.18

Note: All values in cm. Metrics acquired from measurements of structure-from-motion DSMs generated at the Oceano Dunes megaripple stripes. Wavelength measurements for Oceano reported here do not match those reported in Table 1 because these measurements were acquired from different samples and by a different methodology.

The slopes and cross-sectional profiles of features in megaripple corridors are characteristic of megaripples, which have approximately isometric stoss and lee slopes as well as a smaller wavelength-to-height ratio (Zimbelman et al., 2012). The profiles of features in smaller bedform corridors are more typical of impact ripples with shallower stoss slopes and steeper lee slopes. However, the profiles of several bedforms vary from these standards, further suggesting

incomplete sorting of grains between corridor types and a presence of bedforms with intermediate characteristics.

The lowest topographic points in megaripple stripes are megaripple corridor troughs. Megaripple crests represent the highest point in the stripes. The corridors of smaller bedforms are at a height intermediate between the troughs and crests of adjacent megaripple corridors (Figure S7). As these data are only available for one location, it is uncertain if these characteristics are typical of megaripple stripes or incidental. Importantly, these topographic characteristics were also reproduced in modelling of megaripple stripes.

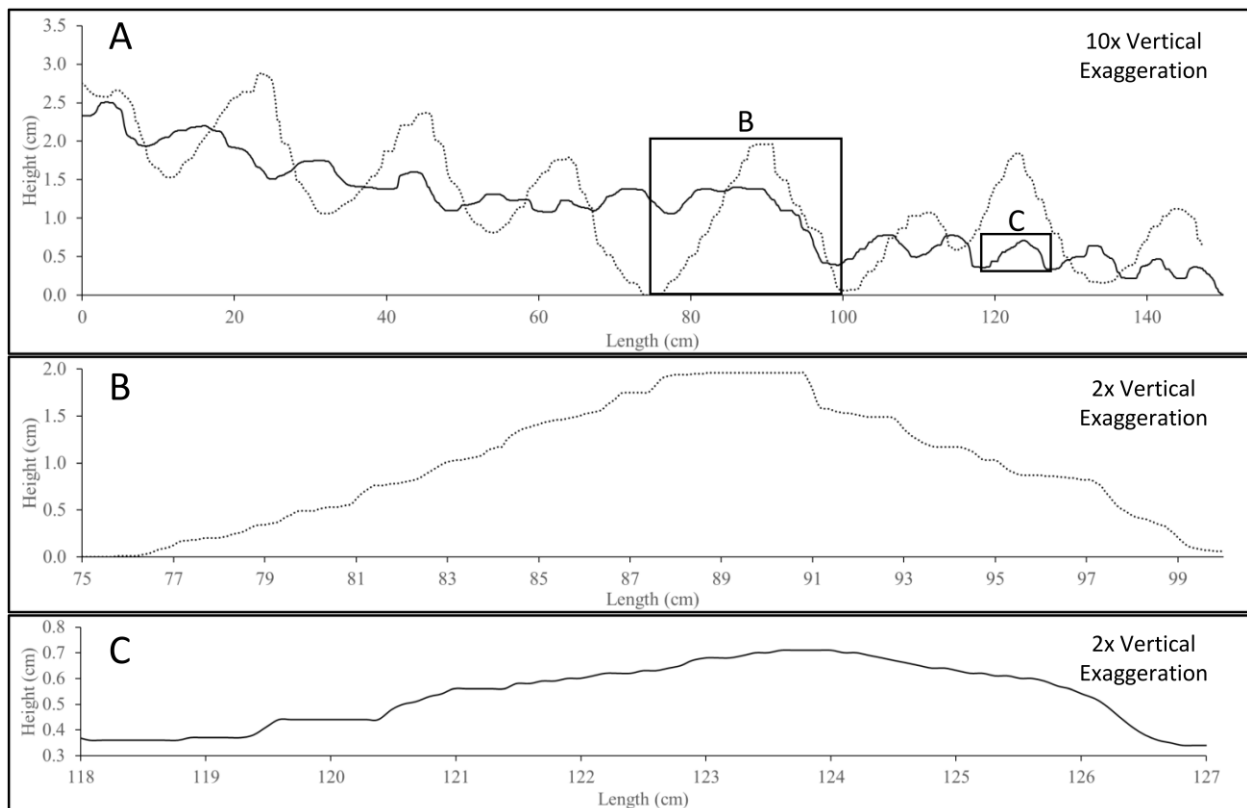


Figure S7: (A) Profile graph of megaripples and smaller bedforms extracted from DSM of stripes at Oceano Dunes, California. Transport direction is left-to-right. Overall, these results show that there are large differences in ripple height and wavelength between corridor types. (B) Inset of megaripple profile. The stoss and lee slopes are of approximately the same length. (C) Inset of smaller bedform profile. The slopes are shallower, and the stoss slope is longer than the lee. Vertical exaggeration in (B) and (C) is 2, giving the same relative scale and allowing for easier comparison of their profiles.

ADDITIONAL TABLES AND FIGURES

TABLE S4. PARAMETERS FOR ALL MEGARIPPLE STRIPE SIMULATIONS

Parameter	Value
Lattice Size	400 x 400, 200 x 800
Initial Sediment Depth	125
Slabs in Model Space	20 000 000
Angle of Repose	30°
Shadow Zone Angle	15°
Slab Aspect Ratio	1:10
Salton, Repton Transport Length	30, 3
Salton, Repton Erosion Probability	1, 0.15
Deposition Probability (All Slabs)	1
Salton, Repton Transport Height (Peak)	200 slabs, 25 slabs

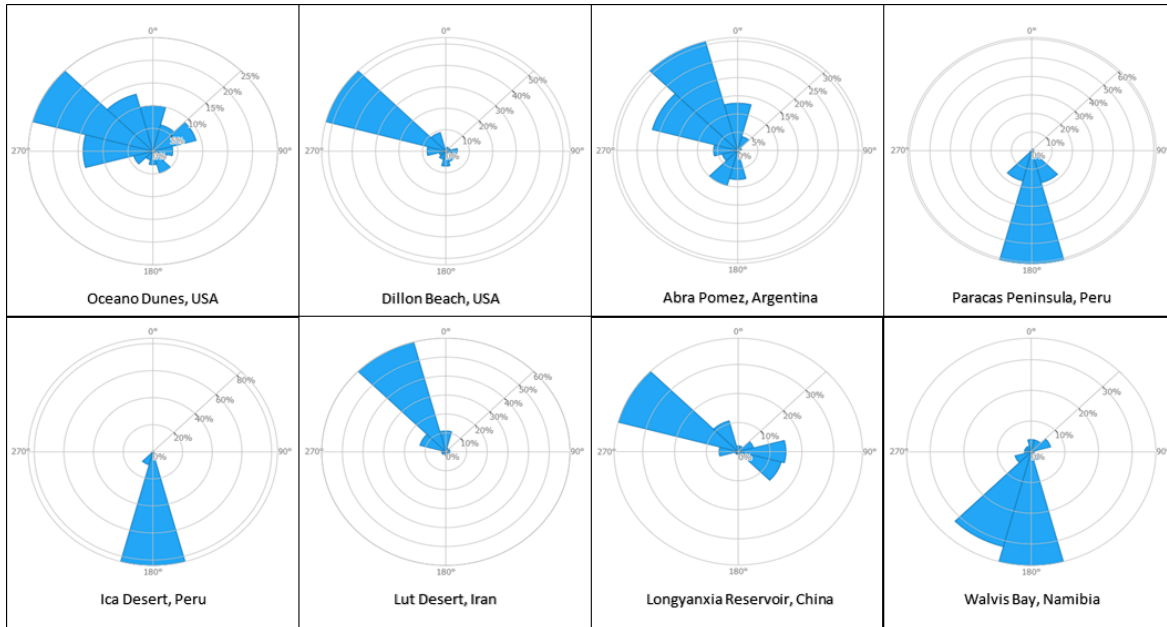


Figure S8: Modelled wind speed roses from Global Wind Atlas for the 8 terrestrial sites listed in Table 1 of the main text. Modelled data are based on ERA5 dataset from the European Centre for Medium-Range Weather Forecasts (ECMWF). Modelled data suggest above-threshold winds are unimodal at all locations. A discussion of the use of modelled wind data for the Puna Plateau in Argentina, where the Abra Pomez megaripple stripes documented here are located, can be found in Favaro et al. (2020).

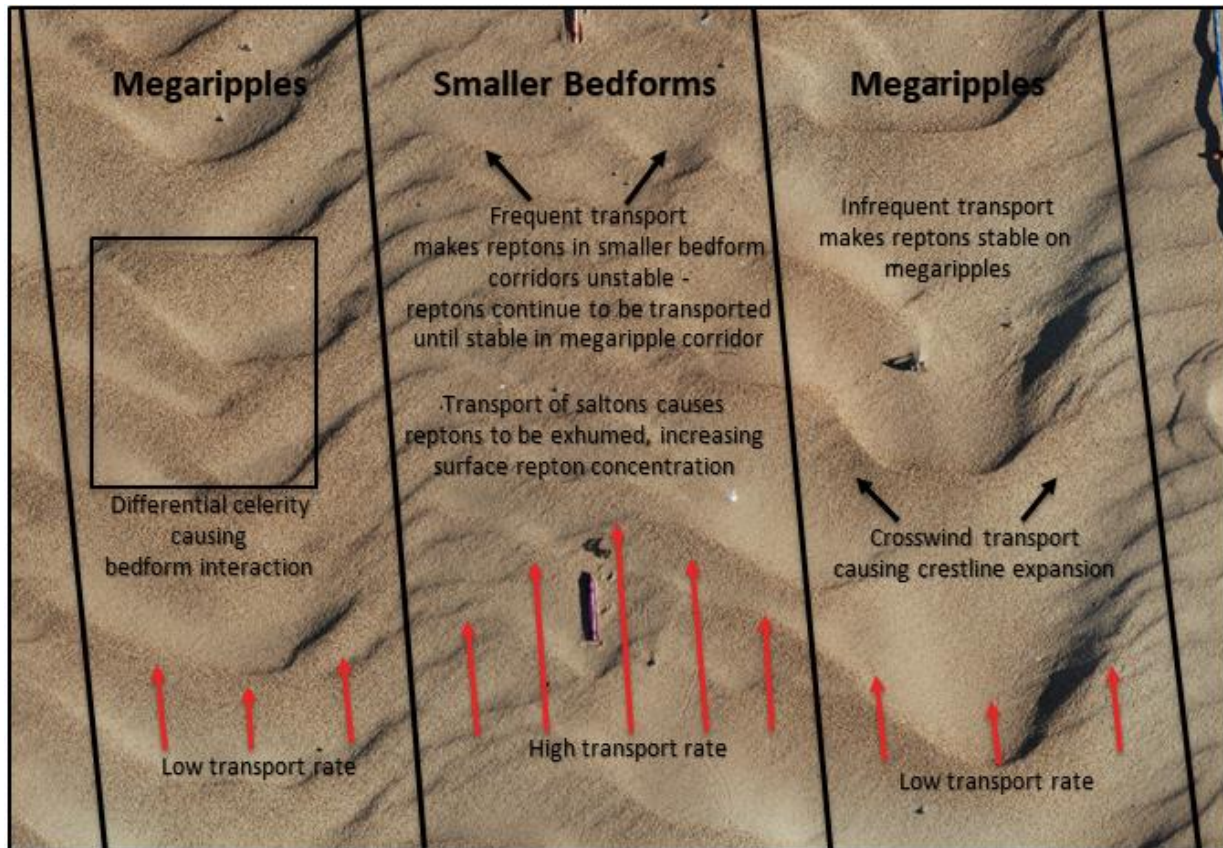


Figure S9: Additional information on small-scale processes hypothesized to affect megaripple stripe formation. Red arrows indicate assumed rate of transport at different locations. Black arrows indicate spanwise transport caused by reptation.

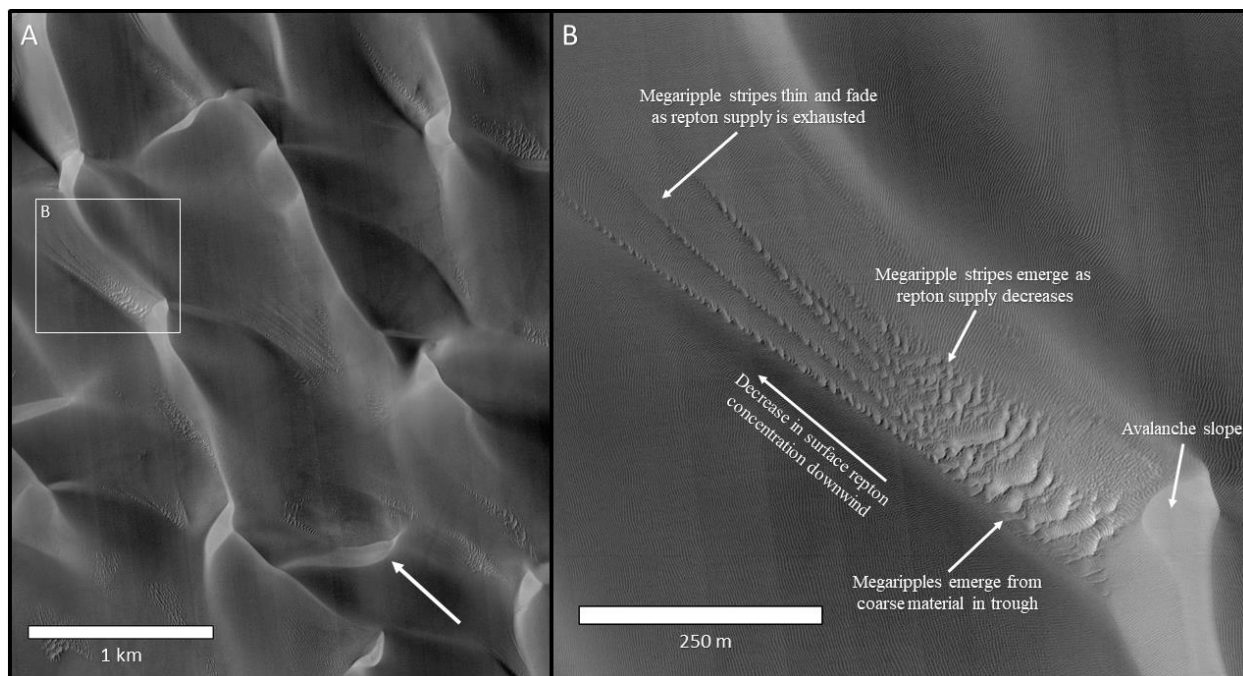


Figure S10: Additional information on large-scale processes hypothesized to affect megaripple stripe formation. (A) Barchanoid dunes and megaripple stripes in Rabe Crater. Megaripple stripes and megaripples have emerged in several locations directly downwind of avalanche slopes and/or from dune troughs. Megaripples extend for some distance and then fade. The dune troughs are likely sources of reptons, which rapidly decrease in availability as the megaripples climb the stoss slopes of dunes. Arrow denotes assumed dominant direction of transport. (B) Inset image with hypothesized downwind decrease in reptons and thinning of the megaripple stripe pattern.

MODEL VIDEOS

4 videos showing development of features in the model space are included in the supplementary material. The parameter being displayed in all simulations is the ‘topslab’, which is the slab type at the surface. In all videos, reptons are red and saltons are yellow (the color ramp is only relevant for the values ‘1.0’ (saltons) and ‘2.0’ (reptons)). The current iteration is visible at the top of the image as “time = ...”.

1. ‘Impact Ripples’. This video shows a 20 000 iteration simulation with a repton concentration of 1.9%. Impact ripples emerge in the simulation and migrate through the model space. No megaripples or megaripple stripes develop in this simulation because of insufficient surface repton concentrations to cause their nucleation.
2. ‘Megaripple Stripes’. This video shows a 20 000 iteration simulation with a repton concentration of 2.5%. The video shows three distinct corridors of megaripples developing as repton concentrations increase. The megaripple corridors widen as more reptons emerge on the surface.
3. ‘Megaripple Stripes 2’. This video shows a 20 000 iteration simulation with a repton concentration of 3.4%. The video shows corridors of megaripples developing more

rapidly and in more locations than at 2.5% repton concentrations. By 10 000 iterations, the corridors of megariipples have merged and the stripes pattern no longer exists. The megariipples coalesce and by iteration 16 000 parts of the basement (red) begin to appear as all available slabs have become part of the megariipples.

4. ‘Megariipples’ This video shows a 20 000 iteration simulation with a repton concentration of 5%. Megariipples begin developing in the model space rapidly, and smaller bedforms do not remain for very long. As with ‘Megariripple Stripes 2’, the basement of the model space becomes exposed as all available mobile slabs become part of the megariipples.

REFERENCES CITED

- Buscombe, D. (2013). Transferable wavelet method for grain-size distribution from images of sediment surfaces and thin sections, and other natural granular patterns. *Sedimentology*, 60(7), 1709-1732, doi:10.1111/sed.12049.
- de Silva, S. L., Spagnuolo, M. G., Bridges, N. T., & Zimbelman, J. R. (2013). Gravel-mantled megariipples of the Argentinean Puna: A model for their origin and growth with implications for Mars. *GSA Bulletin*, 125(11-12), 1912-1929, doi:10.1130/B30916.1.
- Favaro, E. A., Hugenholtz, C. H., Barchyn, T. E., & Gough, T. R. (2020). Wind regime, sediment transport, and landscape dynamics at a Mars analogue site in the Andes Mountains of Northwestern Argentina. *Icarus*, 113765, doi:10.1016/j.icarus.2020.113765
- Francou, B., Méhauté, N. L., & Jomelli, V. (2001). Factors controlling spacing distances of sorted stripes in a low-latitude, alpine environment (Cordillera Real, 16° S, Bolivia). *Permafrost and Periglacial Processes*, 12(4), 367-377, doi:10.1002/ppp.398.
- Hugenholtz, C. H., Barchyn, T. E., & Favaro, E. A. (2015). Formation of periodic bedrock ridges on Earth. *Aeolian Research*, 18, 135-144, doi:10.1016/j.aeolia.2015.07.002.
- Ibbeken, H., & Schleyer, R. (1986). Photo-sieving: A method for grain-size analysis of coarse-grained, unconsolidated bedding surfaces. *Earth Surface Processes and Landforms*, 11(1), 59-77, doi:10.1002/esp.3290110108.
- Jerolmack, D. J., Mohrig, D., Grotzinger, J. P., Fike, D. A., & Watters, W. A. (2006). Spatial grain size sorting in eolian ripples and estimation of wind conditions on planetary surfaces: Application to Meridiani Planum, Mars. *Journal of Geophysical Research: Planets*, 111(E12), doi:10.1029/2005JE002544.
- Lämmel, M., Meiwald, A., Yizhaq, H., Tsoar, H., Katra, I., & Kroy, K. (2018). Aeolian sand sorting and megariripple formation. *Nature Physics*, 14(7), 759-765,

doi:10.1038/s41567-018-0106-z.

- O'Brien, P., & McKenna Neuman, C. (2018). An experimental study of the dynamics of saltation within a three-dimensional framework. *Aeolian Research*, 31, 62-71, doi:10.1016/j.aeolia.2017.09.003.
- Rubin, D. M. (2004). A simple autocorrelation algorithm for determining grain size from digital images of sediment. *Journal of Sedimentary Research*, 74(1), 160-165, doi:10.1306/052203740160
- Vitton, S. J., & Sadler, L. Y. (1997). Particle-size analysis of soils using laser light scattering and X-ray absorption technology. *Geotechnical Testing Journal*, 20(1), 63-73, doi:10.1520/GTJ11421J.
- Weitz, C. M., Sullivan, R. J., Lapotre, M. G., Rowland, S. K., Grant, J. A., Baker, M., & Yingst, R. A. (2018). Sand grain sizes and shapes in eolian bedforms at Gale crater, Mars. *Geophysical Research Letters*, 45(18), 9471-9479, doi:10.1029/2018GL078972.
- Westoby, M. J., Brasington, J., Glasser, N. F., Hambrey, M. J., & Reynolds, J. M. (2012). 'Structure-from-Motion' photogrammetry: A low-cost, effective tool for geoscience applications. *Geomorphology*, 179, 300-314, doi:10.1016/j.geomorph.2012.08.021.
- Yizhaq, H., Isenberg, O., Wenkart, R., Tsoar, H., & Karnieli, A. (2009). Morphology and dynamics of aeolian mega-ripples in Nahal Kasuy, southern Israel. *Israel Journal of Earth Sciences*, 57, 149-165, doi:10.1560/IJES.57.3-4.149.
- Yizhaq, H., Kutra, I., Isenberg, O., & Tsoar, H. (2012a). Evolution of megariipples from a flat bed. *Aeolian Research*, 6, 1-12, doi:10.1016/j.aeolia.2012.05.001.
- Yizhaq, H., Kutra, I., Kok, J. F., & Isenberg, O. (2012b). Transverse instability of megariipples. *Geology*, 40(5), 459-462, doi:10.1130/G32995.1.
- Zimelman, J. R., Williams, S. H., & Johnston, A. K. (2012). Cross-sectional profiles of sand ripples, megariipples, and dunes: a method for discriminating between formational mechanisms. *Earth Surface Processes and Landforms*, 37(10), 1120-1125, doi:10.1002/esp.3243.